



## Research article

# Integrated analysis of differentially expressed genes and miRNA expression profiles in dilated cardiomyopathy

Yu Chen<sup>a,1</sup>, Wen-Ke Cai<sup>b,1</sup>, Jie Yu<sup>b</sup>, Ming Shen<sup>a</sup>, Jin-Huan Zhou<sup>a</sup>, Sheng-Yu Yang<sup>c</sup>, Wei Liu<sup>a</sup>, Si Lu<sup>d</sup>, Yan-Kun Shi<sup>a,\*</sup>, Li-Xia Yang<sup>a,\*\*</sup>

<sup>a</sup> Department of Cardiology, 920th Hospital of Joint Logistics Support Force, PLA, Kunming, China

<sup>b</sup> Department of Thoracocardiac Surgery, 920th Hospital of Joint Logistics Support Force, PLA, Kunming, China

<sup>c</sup> Department of Urology Surgery, 920th Hospital of Joint Logistics Support Force, PLA, Kunming, China

<sup>d</sup> Department of Clinical Medical College, Dali University, Dali, China

## ARTICLE INFO

## Keywords:

Dilated cardiomyopathy  
Genes  
microRNAs  
mRNA-miRNA network  
Bioinformatics

## ABSTRACT

**Background:** Although dilated cardiomyopathy (DCM) is a prevalent form of cardiomyopathy, the molecular mechanisms underlying its pathogenesis and progression remain poorly understood. It is possible to identify and validate DCM-associated genes, pathways, and miRNAs using bioinformatics analysis coupled with clinical validation methods.

**Methods:** Our analysis was performed using 3 mRNA datasets and 1 miRNA database. We employed several approaches, including gene ontology (GO) analysis, KEGG pathway enrichment analysis, protein-protein interaction networks analysis, and analysis of hub genes to identify critical genes and pathways linked to DCM. We constructed a regulatory network for DCM that involves interactions between miRNAs and mRNAs. We also validated the differently expressed miRNAs in clinical samples (87 DCM, 83 Normal) using qRT-PCR.

The miRNAs' clinical value was evaluated by receiver operating characteristic curves (ROCs).

**Results:** 78 differentially expressed genes (DEGs) and 170 differentially expressed miRNAs (DEMs) were associated with DCM. The top five GO annotations were collagen-containing extracellular matrix, cell substrate adhesion, negative regulation of cell differentiation, and inflammatory response. The most enriched KEGG pathways were the Neurotrophin signaling pathway, Thyroid hormone signaling pathway, Wnt signaling pathway, and Axon guidance. In the PPI network, we identified 10 hub genes, and in the miRNA-mRNA regulatory network, we identified 8 hub genes and 15 miRNAs. In the clinical validation, we found 13 miRNAs with an AUC value greater than 0.9.

**Abbreviations:** AUC, area under the curve; BDNF, neurotrophic factor; BP, biological processes; CC, cellular components; DCM, dilated cardiomyopathy; DEG, differentially expressed genes; DEM, differentially expressed miRNA; ECM2, extracellular matrix protein 2; FPR1, Formylated Chemotactic Peptide Receptor 1; GEO, Gene Expression Omnibus; GO, gene ontology; KEGG, Kyoto Encyclopedia of Genes and Genomes, Follicular functions; MCC, Maximum Clique Centrality; mRNA, messenger ribonucleic acid; miRNA, micro ribonucleic acid; PPI, protein-protein interaction; ROC, receiver operating characteristic curve; RRA, RobustRankAggreg (RRA) method; SLRPs, leucine-rich proteoglycans; STRING, Search Tool for the Retrieval of Interacting Genes/Proteins.

\* Corresponding author. Department of Cardiology, 920th Hospital of Joint Logistics Support Force of People's Liberation Army of China Kunming, 212 Daguang Road, Kunming, Yunnan 650032, China.

\*\* Corresponding author.

E-mail addresses: [1103511591@qq.com](mailto:1103511591@qq.com) (Y.-K. Shi), [doctorylixia@aliyun.com](mailto:doctorylixia@aliyun.com) (L.-X. Yang).

<sup>1</sup> These authors contributed equally to this work and share first authorship.

<https://doi.org/10.1016/j.heliyon.2024.e25569>

Received 18 August 2023; Received in revised form 12 January 2024; Accepted 29 January 2024

Available online 12 February 2024

2405-8440/Â© 2024 The Authors. Published by Elsevier Ltd. This is an open access article under the CC BY-NC-ND license (<http://creativecommons.org/licenses/by-nc-nd/4.0/>).

**Conclusion:** Our research offers novel insights into the underlying mechanisms of DCM and has implications for identifying potential targets for diagnosis and treatment of this condition.

### 1. Introduction

Dilated cardiomyopathy is a common cause of heart failure, arrhythmia, and sudden death [1]. Multiple factors, including genetics, non-genetic factors, inflammation, infection, and toxins, contribute to the development of DCM. Furthermore, a person’s genetic profile may influence non-genetic cardiomyopathy, and mixed etiologies may also be present [2].

Heart failure in DCM results from poor performance of the cardiac pump and deficiency of sarcomere contractility [3]. Mutations in genes encoding proteins associated with cytoskeleton, sarcomeres, and mitochondria have been linked to DCM pathogenesis. Accumulating evidence also implicates mutations in desmosomes, nuclear membranes, and RNA binding in DCM development. Truncating variants in Titin(TTN) were found to raise the risk of DCM [2], while missense and truncating variants in Lamin A/C(LMNA) account for 5–8% of the genetic basis of DCM [4]. Genes encoding cardiac cytoskeletal proteins, including Filamin C (FLNC) and Sodium Voltage-Gated Channel Alpha Subunit 5 (SCN5A), as well as proteins involved in sarcomere function, such as Myosin Heavy Chain 7 (MYH7), Troponin T2(TNNT2), and Tropomyosin 1(TPM1), have been found to be involved in DCM [5].

MicroRNAs (miRNAs) are RNA molecules that are single-stranded and composed of approximately 19–25 nucleotides. Recent studies have demonstrated the crucial role of miRNAs in the pathogenesis of dilated cardiomyopathy (DCM). One study reported the relationship between myocardial fibrosis and cardiac miRNA in DCM, discussing the role of miRNA in DCM and its potential as therapeutic targets [6]. Another study utilized integrative analysis to identify miRNA-mRNA interactions in pediatric DCM [7]. Overall, miRNAs play a significant role in the pathogenesis of DCM and holds promise as potential therapeutic targets.

Despite significant advancements in understanding DCM, several challenges remain. Firstly, early diagnosis remains difficult, resulting in high mortality rates, as no early diagnostic biomarkers are currently available. Secondly, there are no specific curative or alleviative treatments; only basic therapies targeting heart failure are available. Therefore, molecular mechanisms underlying the disease need to be better understood. Recent breakthroughs in microarray technology and bioinformatics analysis have ushered in a new era for DCM research. The ability to identify gene mutations and accurately locate DCM-associated genomic regions and functional pathways at the genomic level has opened exciting new avenues for investigation. In cardiovascular research, obtaining in vivo tissue samples in clinical settings is challenging. There is increasing interest in using circulating miRNAs as biomarkers for disease diagnosis since they are easy to detect, relatively stable, and tissue-specific. Furthermore, the interactions between miRNAs and mRNAs can help elucidate the intricate mechanisms of DCM.

We identified differentially DEGs by analyzing three DCM mRNA datasets from the Gene Expression Omnibus (GEO) microarray platform and DEMs from one DCM miRNA dataset on the GEO microarray platform. Utilizing GO, KEGG, and PPI pathway analysis, we

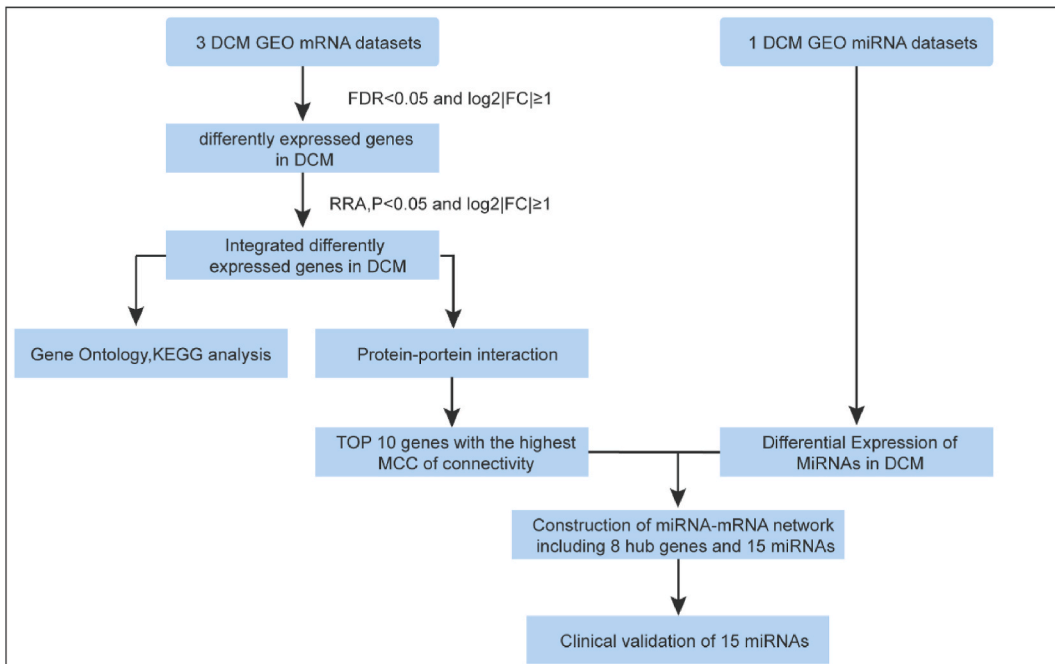


**Fig. 1.** This is the flowchart for the study. DCM, dilated cardiomyopathy; DEGs, differentially expressed genes; KEGG, Kyoto Encyclopedia of Genes and Genomes; PPI, protein-protein interaction; RRA, Robust Rank Aggregation.

aimed to pinpoint key genes and pathways. To further understand the molecular mechanisms of DCM, we established a miRNA-mRNA network. Clinical validation of the microarray results was conducted by examining miRNA levels in the serum of patients with DCM. Additionally, we assessed the diagnostic performance of each miRNA using Receiver Operating Characteristic (ROC) curve analysis (Fig. 1).

## 2. Methods

### 2.1. Microarray data

Data from GEO were utilized in the study, including gene expression datasets (GSE1145, GSE29819, and GSE141910), and microRNA expression dataset (GSE209991) (Table S1, Supplementary file). Samples were obtained from cardiac surgery patients undergoing heart transplants, and control samples were obtained from donor hearts that had not been used. Information pertaining to DCM and normal cardiac tissue was extracted from the datasets for subsequent analysis. Clinical background information for the populations analyzed was provided by the original citation for GSE29819 [8], while for GSE141910, clinical background information was summarized (Table S2, Supplementary file) since the publication had not yet been released. There was no clinical information available for the samples included in GSE1145. The datasets contained varying numbers of DCM tissue and normal tissue samples, with the GSE141910 dataset having the largest sample size. The GSE209991 dataset included ten plasma samples from DCM and ten plasma samples from normal.

### 2.2. Differentially expressed gene screening

DEGs were analyzed using limma (ver 3.52.2) in R version 4.2.0. DEGs were analyzed using limma (ver 3.52.2) in R version 4.2.0, with selection criteria of  $P < 0.05$  and  $|\log_2FC| \geq 1$ . We generated a candidate gene list to distinguish DCM from normal tissue using the RRA method in R language, with a threshold of  $P < 0.05$ . The comprehensive list of DEGs was used for subsequent analyses.

### 2.3. KEGG and GO enrichment analysis of DEGs

With a view to improving our understanding of DEGs' biological functions and pathways, we performed functional enrichment analysis using Metascape [9]. Metascape is a powerful tool that integrates information from over forty independent sources into a single platform, including GO and KEGG databases [10]. The GO database provides comprehensive gene functional annotations, including three domains: biological process (BP), molecular function (MF), and cellular component (CC) [11]. We performed Metascape analysis on the DEGs using parameters with a minimum overlap of 3, a minimum enrichment factor of 1.5, and a significance threshold of  $P < 0.05$ .

### 2.4. Protein-protein interaction network construction and hub gene analysis

This study used the Search Tool for the Retrieval of Interacting Genes/Proteins (STRING) database to analyze protein-protein interactions [12]. This database integrates publicly available information on protein-protein interactions and incorporates computational predictions [13]. PPIs were mapped to known integrated DEGs, and statistics were considered significant when the interaction score exceeded 0.4. Cytoscape enables additional data to be imported into networks and presented visually in a more flexible way, making it a powerful tool for analyzing and visualizing large-scale networks [14]. Based on Maximum Clique Centrality (MCC), we identified the top ten central genes using the CytoHubba plugin in Cytoscape [15].

### 2.5. Identification of DEMs (differential expression of MiRNAs)

We utilized the R package "Limma" to generate an expression matrix for probe genes and to analyze the GSE209991 dataset. Next, the probes were converted into genetic symbols that corresponded to the probes. Additionally, using the "Limma" package, we calculated P values for DEGs between DCM and normal samples. To screen for differentially expressed miRNAs, we used the criteria of  $P < 0.05$  and  $|\log_2FC| \geq 1$ .

### 2.6. DEMs target genes prediction and construction of miRNA-mRNA network

MultiMiR (<http://multimir.org>) is an excellent source of information regarding miRNA-target interactions [16]. In this study, we utilized the multiMiR package (version 1.18.0) to retrieve interactions between DEMs and hub genes. To construct an interaction network between DEMs and DEGs based on miRNAs and mRNAs, we further analyzed the DEMs and DEGs using Cytoscape.

### 2.7. Clinical validation

**Participants.** In this study, we utilized a cross-sectional research design. Samples were collected from January 2023 to April 2023 at 920th Hospital of Joint Logistics Support Force, including patients diagnosed with DCM and normal individuals. The inclusion criteria for DCM were patients clinically diagnosed with DCM and excluded from other diseases that require differential diagnosis, such

as valvular disease, hypertensive heart disease, and ischemic cardiomyopathy. The inclusion criteria for normal individuals were ordinary patients with no abnormalities detected by cardiac ultrasound. Ultimately, 87 normal individuals and 83 DCM patients were sampled ( Table S7, Supplementary file ).

**RT-qPCR analysis.** In this experiment, stem-loop reverse transcription [17] was used to synthesize cDNA from miRNAs, and the TaqMan MicroRNA Reverse Transcription Kit (Thermo Fisher Scientific, USA) was employed. Subsequently, qRT-PCR was performed using TaqMan MicroRNA Assays (20x) (Thermo Fisher Scientific, USA) and TaqMan 2 × Universal PCR Master Mix (Thermo Fisher Scientific, USA) (Table S8, Supplementary file). In order to normalize serum miRNA expression levels, U6 (Takara, Japan) was used for normalization. To ensure consistency of all measured results, the internal controls for each PCR amplification reaction consisted of three independent RNA samples. To compare DCM samples and normal samples,  $-\Delta\Delta\text{Ct}$  values were calculated, which allowed us to determine the relative expression levels of miRNAs. The fold change in miRNA expression has been calculated using the  $2^{-\Delta\Delta\text{Ct}}$  method and each sample was calculated three times [18].  $\Delta\Delta\text{Ct} = [(Ct_{\text{miRNA}} - Ct_{\text{U6}})_{\text{DCM}} - (Ct_{\text{miRNA}} - Ct_{\text{U6}})_{\text{normal}}]$ .

**ROC curves.** ROC curves were constructed for each miRNA, and AUC values were analyzed to determine their diagnostic performance. The relative expression level was calculated using  $-\Delta\Delta\text{Ct}$ , and if the expression level was 0,  $-\Delta\Delta\text{Ct}$  was defined as  $-100$ . We used the pROC package in R (version 4.2.0) to conduct the statistical analysis.

## 2.8. Statistical analysis

Frequency and proportion were used to describe categorical variables, whereas median (interquartile range) or mean (standard deviation) were used to describe continuous variables. Wilcoxon Mann-Whitney test (for continuous variables) or Fisher exact test (for categorical variables) were used to compare the distributions of variables between the DCM group and the Normal group. R (version 4.2.0) was used for all statistical analyses.

## 3. Results

### 3.1. Identification of DEGs

In the GSE1145 database, 966 DEGs were identified, 413 of which were upregulated and 553 of which were downregulated, where the expression changes in DCM tissue were two-fold or greater compared to the control group. (Figs. 2A and 3A). Similarly, based on the GSE29819 database, the expression changes of 905 DEGs were found to be double or more than double in DCM tissues, with 439 upregulated and 466 downregulated (Figs. 2B and 3B). In the GSE141910 database, the expression changes of 954 DEGs were found to be double or more than double in DCM tissues compared to controls, with 543 upregulated and 411 downregulated (Figs. 2C and 3C). Finally, the RobustRankAggreg (RRA) method was used to rank the importance of genes across the three chips, resulting in the identification of 48 genes that have been upregulated and 30 genes that have been downregulated (Fig. 3D, additional file1, Table S3).

### 3.2. Gene function and pathway enrichment analysis

We used Metascape to perform GO annotation (Fig. 4A, Table S4) and KEGG pathway enrichment analysis (Fig. 4B–Table S5) on the integrated DEGs. The enrichment background consisted of all genes present in the genome. Grouping was based on similarity, with those having P-values less than 0.05, enrichment scores greater than 1.5, and minimum counts of 3 being grouped together. The GO annotation analysis produced extensive data, with the most prominent biological processes being collagen-containing extracellular matrix, cell-substrate adhesion, negative regulation of cell differentiation, and inflammation, as shown in the top four terms. The

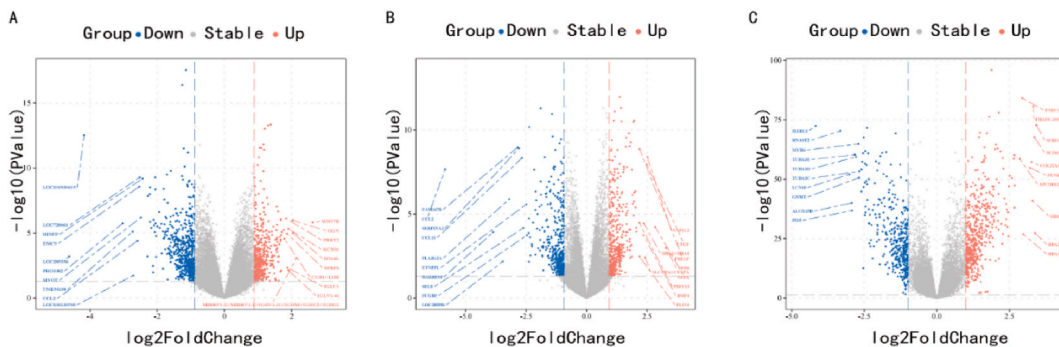


**Fig. 2.** Volcano plots were utilized to perform differential expression analysis of DEGs from GSE1145, GSE29819, and GSE141910 datasets. The volcano plot of GSE1145 (A) showed that compared to the control group, there were 413 upregulated and 553 downregulated genes with expression changes of at least 2-fold. Similarly, the volcano plot of GSE29819 (B) revealed 439 upregulated and 466 downregulated genes. Finally, the volcano plot of GSE141910 (C) displayed 543 upregulated and 411 downregulated genes. The colored dots corresponding to upregulation, downregulation, and no significant change in mRNA are indicated by red, blue, and grey dots respectively. (For interpretation of the references to color in this figure legend, the reader is referred to the Web version of this article.)

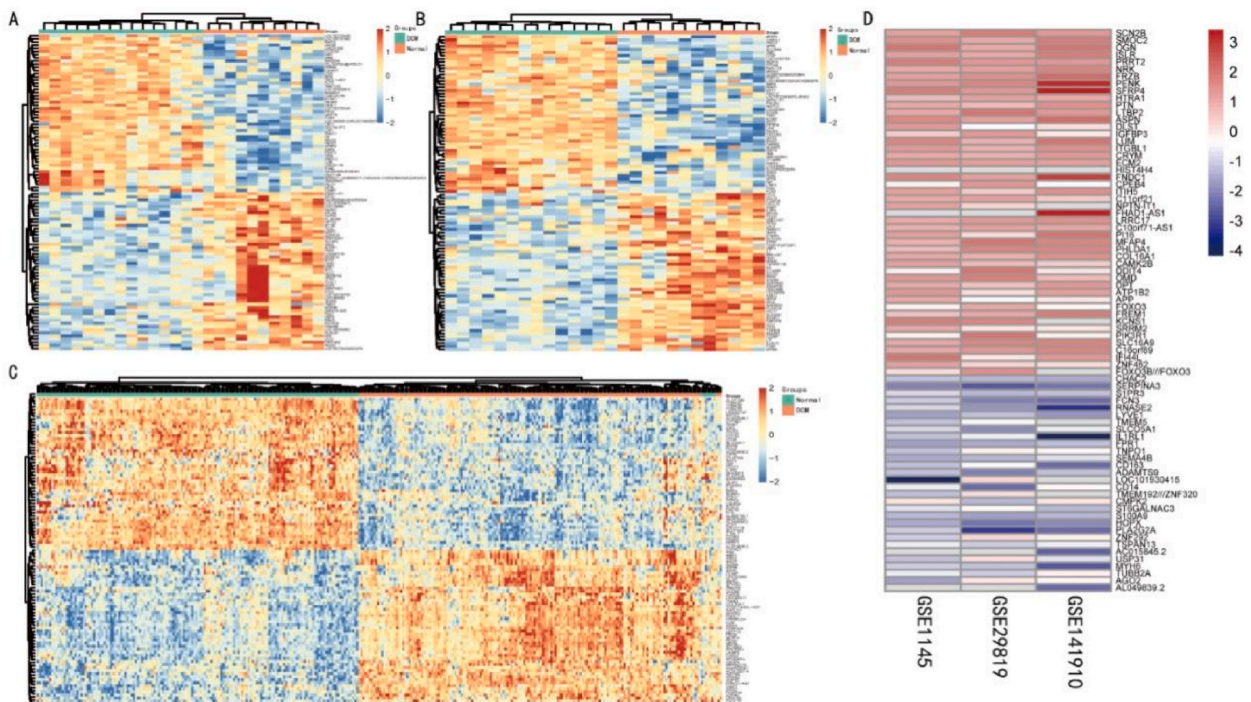


**Fig. 3.** DEG heatmaps for GSE1145, GSE29819, and GSE141910. (A) GSE1145, (B) GSE29819, (C) GSE141910, (D) RobustRankAggreg (RRA) of three mRNA datasets. A–C: Green, DCM; Red, normal heart tissues. A–D: Red color was used to depict the upregulated genes, while blue color was used to depict the downregulated genes. (For interpretation of the references to color in this figure legend, the reader is referred to the Web version of this article.)

Metascape database showed that the Neurotrophin signaling pathway, Thyroid hormone signaling pathway, Wnt pathway, and Axon guidance pathway were the top KEGG pathways. To calculate p-values, we used a cumulative hypergeometric distribution, while a Benjamini-Hochberg procedure was applied to calculate q-values to prevent the possibility of multiple testing bias [19].

We utilized a similarity metric of Kappa scores for hierarchical clustering of enriched terms, with clusters defined as subtrees having a similarity greater than 0.3. The term that showed the highest level of statistical significance within a cluster represented it. The nodes in Fig. 4C were colored according to their cluster affiliation. A stronger correlation was observed among terms within the same cluster. In Fig. 4D, we observed that the degree of enrichment (represented by color) increased with an increase in the number of genes included. The more genes that were included, the greater the degree of enrichment observed.

### 3.3. PPI network and hub genes

We analyzed physical PPIs among the 78 DCM nodes using STRING version 11.5. We utilized the cytoHubba plugin in Cytoscape software and used MCC algorithm to determine hub genes (Fig. 5A). Our analysis identified 10 genes (OGN, ASPN, DPT, LUM, OMD, ECM2, CD14, MFAP4, S100A9, and FPR1) with the highest scores as hub genes (Fig. 5B), suggesting their potential involvement in progression of DCM. Among the 10 hub genes, seven were upregulated (OGN, ASPN, DPT, LUM, OMD, MFAP4, and ECM2), and three were downregulated (CD14, S100A9, and FPR1).

### 3.4. Identification of DEMs and miRNA-mRNA network construction

In the GSE209991 miRNA database, a significant difference ( $|\log_2FC| > 1$ ) was observed in expression levels between DCM and control tissues (Fig. 6A and B) with 41 miRNAs upregulated and 129 miRNAs downregulated.

The potential interactions between hub genes and differentially expressed miRNAs (DEMs) were determined by analyzing the DEM and hub gene data using the R package multiMiR. In our analysis, 15 miRNAs were detected as differentially expressed, including hsa-miR-124-3p, hsa-miR-1976, hsa-miR-483-3p, and hsa-miR-486-5p with upregulated expression, as well as hsa-miR-26b-5p, hsa-miR-98-5p, hsa-miR-20a-5p, hsa-miR-361-5p, hsa-miR-379p, hsa-miR-449a, hsa-miR-286-5p, and hsa-miR-454-3p with downregulated expression in DCM tissues compared to control tissues. Furthermore, eight mRNAs were identified, including upregulated ASPN, DPT, ECM2, LUM, MFAP4, and OMD, and downregulated CD14 and FPR1. The strength of interaction between miRNAs and mRNAs was shown in Table S6. Subsequently, we used Cytoscape to construct a miRNA-mRNA network (Fig. 6C), which suggested potential interactions between DE miRNAs and hub genes.

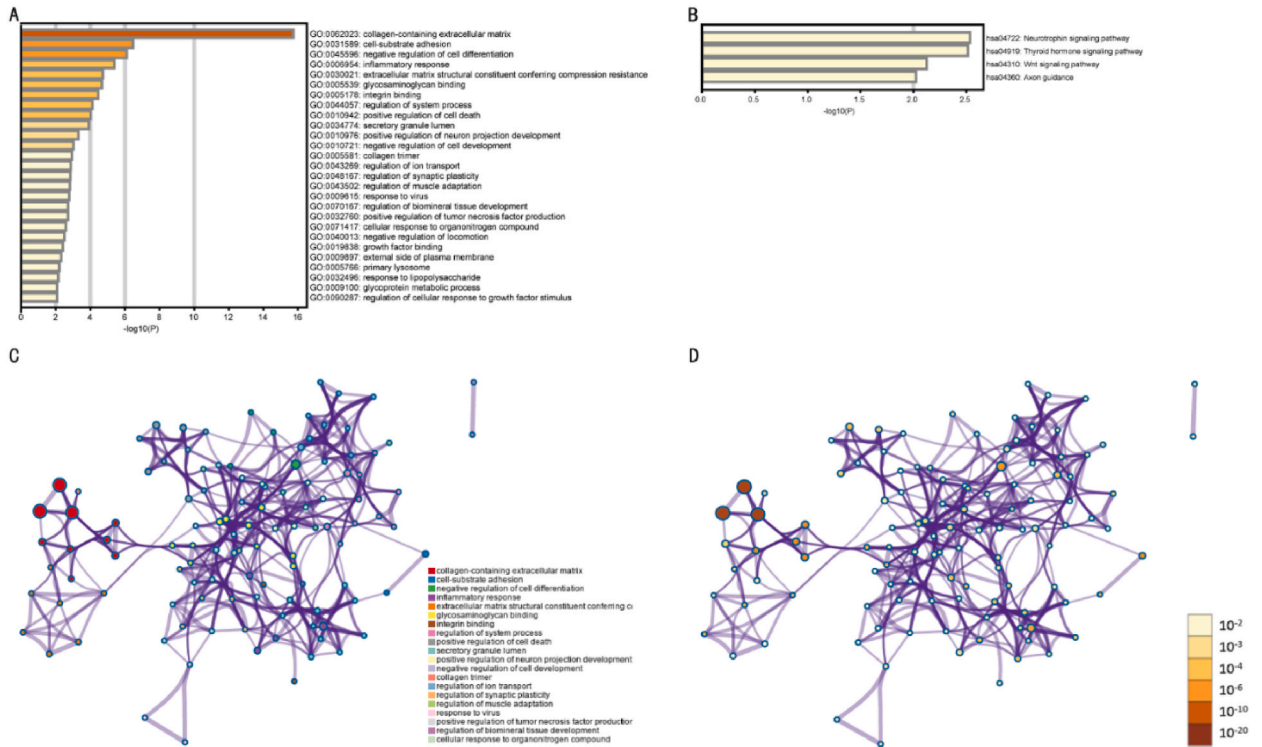


**Fig. 4.** Statistical analysis of functional enrichment of DEGs. Bar charts were used to present top 20 results of GO enrichment analysis (A) and KEGG enrichment analysis (B), with P-values. The merged representation of panels C and D from the Metascape analysis shows the clustering of differentially expressed genes according to GO and KEGG pathways, where the color coding in panel C indicates the categorization of each gene within these classifications, and in panel D, the color intensity reflects the p-value significance of each gene. (For interpretation of the references to color in this figure legend, the reader is referred to the Web version of this article.)

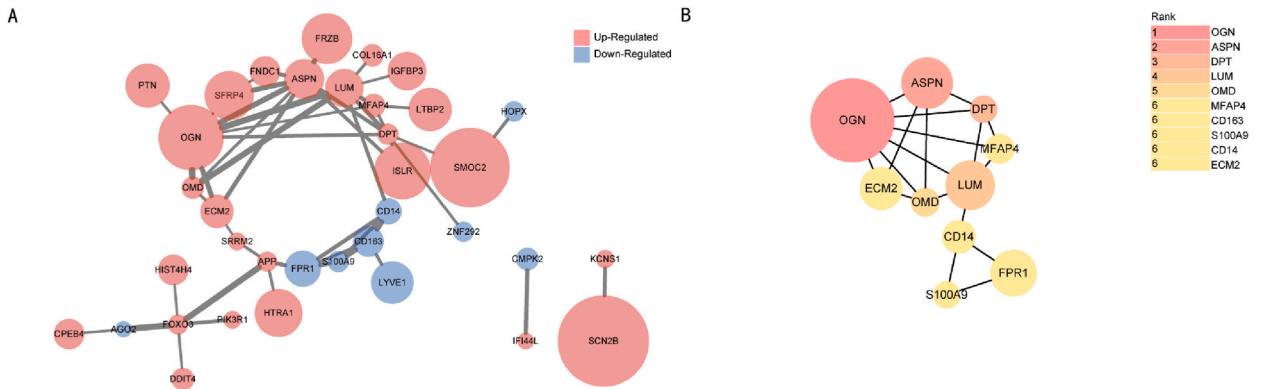


**Fig. 5.** An integrated PPI network has been constructed using DEGs and hub genes. (A) displayed all interactions between the integrated DEGs, with red and blue nodes representing upregulated and downregulated genes, respectively. (B) displayed the top 10 hub genes. (For interpretation of the references to color in this figure legend, the reader is referred to the Web version of this article.)

3.5. Clinical validation

The expression levels of miRNAs obtained from bioinformatics analysis were quantified using qRT-PCR for clinical validation (Table 1). By analyzing the AUC value of the DEMs (Fig. 7), we evaluated their potential to serve as biomarkers for DCM for the DCM and Normal groups. Except for hsa.miR.483.3p and has.miR.124.3p, all other AUC values were greater than 0.9. These miRNAs have extremely high clinical application potential.

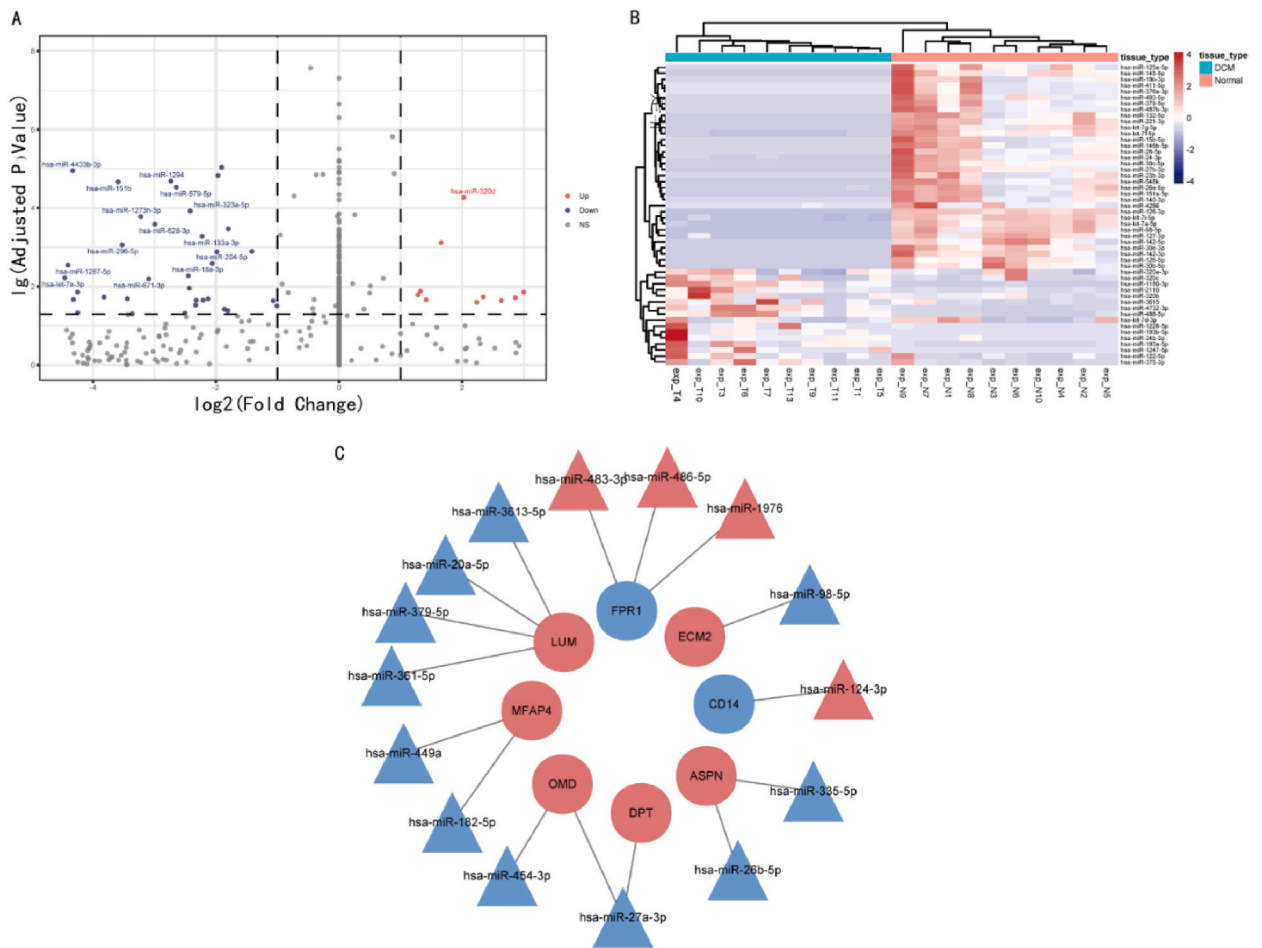


**Fig. 6.** The miRNA dataset GSE209991 was analyzed to generate volcano plots and heat maps of DEMs. (A) The volcano plots displayed 41 miRNAs that were upregulated (represented by red dots), 129 miRNAs that were downregulated (represented by blue dots), and miRNAs that did not show significant changes (represented by grey dots). (B) The DE-miRNAs were presented in a heatmap. (C) A regulatory miRNA-mRNA network was generated, where upregulated miRNAs were represented by blue and downregulated miRNAs were represented by red. (For interpretation of the references to color in this figure legend, the reader is referred to the Web version of this article.)

#### 4. Discussion

The aim of this investigation was to unveil the molecular underpinnings of DCM by harnessing the power of bioinformatics tools to uncover DEGs, enriched pathways, and hub genes, as well as to unveil the intricate miRNAs-mRNAs regulatory network associated with these hub genes. Our meticulous analysis unearthed a striking repertoire of 78 DEGs, with 4 top GO annotations, and 4 KEGG pathways that were significantly enriched in DCM. Additionally, we meticulously constructed a complex regulatory network, comprising 8 hub genes and 15 miRNAs, that were deemed central to the pathogenesis of DCM. Also, 13 DEMs with an AUC greater than 0.9 were validated clinically.

Gene ontology (GO) enrichment analysis revealed significant changes in extracellular matrix modules. The extracellular matrix (ECM) remodeling and fibrosis seen in DCM involves multiple pathways and processes [20]. The structural ECM components that confer tissue integrity become altered, including collagens, proteoglycans, and glycoproteins. This leads to abnormal cell-matrix interactions mediated by integrins and dystroglycan complexes that connect the cytoskeleton to the ECM. The binding of cells to an overly rigid ECM due to increased collagen deposition activates mechanosensitive signaling pathways like integrin/FAK/Src and RhoA/ROCK, resulting in further fibrotic changes. The neurotrophin signaling pathway, activated by BDNF, regulates tissue fibrosis. BDNF binds TrkB receptors, activating PI3K/Akt and MEK/ERK signaling. These pathways inhibit apoptosis and fibrosis while promoting angiogenesis [21]. The Wnt/ $\beta$ -catenin pathway also regulates fibrosis. Wnt binds Frizzled receptors, inhibiting GSK3 $\beta$  activity. This prevents  $\beta$ -catenin degradation, allowing its nuclear translocation and activation of gene expression. Wnt signaling reduces matrix metalloproteinases to inhibit fibrosis [22]. Thyroid hormones act on cardiomyocytes through thyroid receptors to regulate metabolism, apoptosis, and fibrosis. Thyroid hormone therapy has been shown to improve cardiac function in DCM in clinical studies [23]. Axon guidance pathways like Slit-Robo, Ephrins-Eph, and Semaphorins-Plexins regulate neural development but also play roles in the

**Table 1**  
The expression levels of DE-miRNAs in the serum of the DCM and Normal groups.

	Normal N = 87	DCM N = 83	p.overall
hsa.miR.26b.5p	12.3 [10.1; 13.1]	5.29 [4.81; 5.49]	<0.001
hsa.miR.335.5p	7.38 [3.91; 8.53]	-100.00 [-100.00; -100.00]	<0.001
hsa.miR.124.3p:			<0.001
-100	87 (100%)	61 (73.5%)	
0	0 (0.00%)	22 (26.5%)	
hsa.miR.27a.3p	14.0 [12.3; 15.2]	6.27 [6.04; 9.01]	<0.001
hsa.miR.98.5p	14.9 [14.5; 15.1]	6.94 [3.70; 8.55]	<0.001
hsa.miR.1976	-100.00 [-100.00; 100.00]	1.58 [0.00; 4.17]	<0.001
hsa.miR.483.3p:			<0.001
-100	42 (48.3%)	55 (66.3%)	
0	45 (51.7%)	13 (15.7%)	
1	0 (0.00%)	9 (10.8%)	
2	0 (0.00%)	6 (7.23%)	
hsa.miR.486.5p	11.7 [10.8; 11.8]	13.7 [13.5; 14.9]	<0.001
hsa.miR.20a.5p	7.29 [4.32; 9.42]	2.00 [1.00; 3.00]	<0.001
hsa.miR.361.5p	6.61 [4.81; 8.60]	0.00 [-100.00; 2.00]	<0.001
<b>hsa.miR.3613.5p</b>	9.09 [7.63; 9.65]	1.00 [1.00; 3.70]	<0.001
<b>hsa.miR.379.5p</b>	10.6 [9.98; 12.6]	1.00 [0.00; 3.81]	<0.001
hsa.miR.182.5p	9.34 [8.08; 10.5]	4.25 [4.00; 6.09]	<0.001
hsa.miR.449a	7.01 [6.27; 7.46]	2.58 [2.32; 3.00]	<0.001
hsa.miR.454.3p	7.19 [3.81; 8.85]	0.00 [-100.00; 1.58]	<0.001

The unit for quantification of miRNA expression is  $-(\Delta\Delta Ct)$ , and  $2^{-(\Delta\Delta Ct)}$  is used to represent the relative expression level. If the expression of a miRNA was not detected,  $-(\Delta\Delta Ct)$  is defined as  $-100$ .

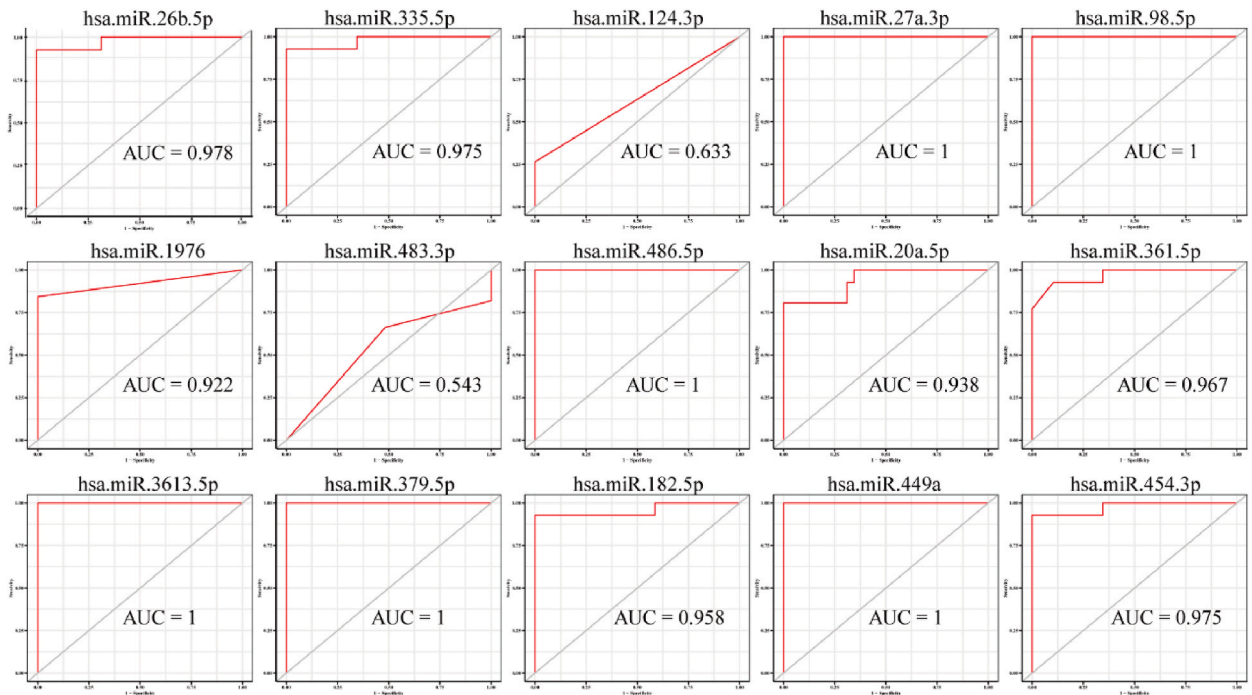


**Fig. 7.** ROC of De-miRNAs. AUC, area under the curve; ROC, receiver operating characteristic curves.

cardiovascular system. They modulate angiogenesis and vascular development through crosstalk with integrins [24]. Their roles in DCM remodeling are still being elucidated but they represent intriguing new pathways. In summary, the enriched pathways highlight the importance of cell-matrix interactions, mechanosignaling, apoptosis, metabolism, angiogenesis, and neural-cardiac crosstalk in the molecular processes underlying DCM pathogenesis. Targeting these pathways therapeutically may attenuate the adverse remodeling in DCM.

The top ten DEGs were identified as hub genes with an MCC Score  $\geq 7$ . The upregulated mRNAs identified, including ASPN [25], OGN [26], LUM [27], OMD [28], DPT [29], ECM2 [30], and MFAP4 [31], are involved in extracellular matrix (ECM) regulation and

fibrosis. Accumulation of ECM is a key process in cardiac fibrosis and progression of DCM. The downregulated mRNAs, including S100A9 [32], CD14 [33], and FPR1 [34], are involved in reducing ECM, inflammation, and chemotaxis. Their downregulation may contribute to ECM accumulation in DCM.

Several miRNAs were found to target and regulate these mRNAs. The downregulation of miR-335-5p, miR-26b-5p, miR-3613-5p, miR-20a-5p, miR-379-5p, and miR-361-5p may relieve inhibition on profibrotic ECM mRNAs OGN, LUM, and OMD, allowing their upregulation. The downregulation of miR-454-3p and miR-27a-3p may relieve inhibition of OMD and DPT. Downregulation of miR-449a and miR-182-5p removes inhibition of MFAP4, enabling its upregulation. The downregulation of miR-98-5p relieves inhibition of ECM2. Finally, downregulation of miR-124-3p, miR-483-3p, miR-486-5p, and miR-1976 removes inhibition of CD14 and FPR1.

Overall, the dysregulation of these miRNA-mRNA networks promotes ECM accumulation, cardiac fibrosis, hypertrophy, and cell death in DCM by removing inhibition on profibrotic mRNAs and enabling their upregulation. Further research on these networks and discovery of additional miRNA-mRNA interactions will provide greater insight into DCM pathogenesis and potentially uncover novel therapeutic targets.

## 5. Limitations

DCM is a complex disorder influenced by various microRNAs, genes, pathways, and their regulatory relationships. Although some miRNAs have been identified as potential biomarkers for DCM, the precise mechanism of their action remains unclear. Further studies with multi-stage samples are needed to validate the results. In addition, the in-silico approach has intrinsic limitations compared to experimental validations. Follow-up functional studies are required to unravel the intricate gene regulatory network governing DCM pathogenesis.

Specifically, the DCM samples used in the bioinformatics analysis were obtained from the myocardium of NYHA IV stage patients during heart transplantation, while the miRNA samples used for clinical validation were obtained from patients in NYHA II-IV stages. Therefore, the generalizability of our conclusions regarding DEGs, hubgenes, and GO/KEGG pathways is limited to the end-stage of DCM.

## 6. Conclusion

We investigated the progression of DCM by integrating three gene expression datasets and a miRNA expression dataset, identifying 78 DEGs, 10 hub genes, and 13 DEMs that may serve as potential diagnostic and therapeutic targets. DCM is a complex disease that is regulated by multiple functions and pathways, highlighting the importance of investigating the interactions between miRNAs, mRNAs, and pathways in the regulation of DCM. In particular, hsa.miR.379.5p, hsa.miR.3613.5p and LUM stand out for their importance and involvement in our study as potential diagnostic or prognostic markers for DCM, warranting future translational research and clinical validation. Future directions include utilizing experimental models to delve deeper into the identified key molecular networks in DCM, as well as integrating with clinical phenotypic data, to provide valuable insights into DCM pathogenesis, biomarker discovery, and personalized therapeutics. We believe this study lays the foundation for translational research on DCM.

## Ethics approval and consent to participate

In accordance with the ethical guidelines of the Helsinki Declaration, the experimental protocol was developed and approved by the Human Ethics Committee of the 920th Hospital of the Joint Logistics Support Force. (Lot no.2023-85-01). Written informed consent was obtained from individual or guardian participants.

## Data availability

Data will be made available on request.

## Funding

This study was funded by Joint Special Fund for Application and Basic Research of Kunming Medical University(202201AY070001-290).

## CRedit authorship contribution statement

**Yu Chen:** Visualization, Project administration, Methodology, Conceptualization. **Wen-Ke Cai:** Supervision, Conceptualization. **Jie Yu:** Writing – original draft, Methodology, Investigation. **Ming Shen:** Writing – review & editing, Methodology, Investigation. **Jin-Huan Zhou:** Investigation. **Sheng-Yu Yang:** Supervision. **Wei Liu:** Resources. **Si Lu:** Investigation. **Yan-Kun Shi:** Writing – review & editing, Project administration, Methodology, Conceptualization. **Li-Xia Yang:** Writing – review & editing, Supervision.

## Declaration of competing interest

The authors declare that they have no known competing financial interests or personal relationships that could have appeared to

influence the work reported in this paper.

## Acknowledgements

Not applicable.

## Appendix A. Supplementary data

Supplementary data to this article can be found online at <https://doi.org/10.1016/j.heliyon.2024.e25569>.

## References

- [1] S. Heymans, et al., Dilated cardiomyopathy: causes, mechanisms, and current and future treatment approaches, *Lancet* 402 (10406) (2023) 998–1011.
- [2] E.M. McNally, L. Mestroni, Dilated cardiomyopathy: genetic Determinants and mechanisms, *Circ. Res.* 121 (7) (2017) 731–748.
- [3] A.V. Dvornikov, P.P. de Tombe, X. Xu, Phenotyping cardiomyopathy in adult zebrafish, *Prog. Biophys. Mol. Biol.* 138 (2018) 116–125.
- [4] S. Crasto, I. My, E. Di Pasquale, The Broad Spectrum of LMNA cardiac diseases: from molecular mechanisms to clinical Phenotype, *Front. Physiol.* 11 (2020) 761.
- [5] J. Lukas Laws, et al., Arrhythmias as Presentation of genetic cardiomyopathy, *Circ. Res.* 130 (11) (2022) 1698–1722.
- [6] E. Alonso-Villa, et al., The role of MicroRNAs in dilated cardiomyopathy: new insights for an Old entity, *Int. J. Mol. Sci.* 23 (21) (2022).
- [7] F.T. Hailu, et al., Integrated analysis of miRNA-mRNA interaction in pediatric dilated cardiomyopathy, *Pediatr. Res.* 92 (1) (2022) 98–108.
- [8] A. Gaertner, et al., Myocardial transcriptome analysis of human arrhythmogenic right ventricular cardiomyopathy, *Physiol. Genom.* 44 (1) (2012) 99–109.
- [9] Y. Zhou, et al., Metascape provides a biologist-oriented resource for the analysis of systems-level datasets, *Nat. Commun.* 10 (1) (2019) 1523.
- [10] M. Kanehisa, et al., KEGG: new perspectives on genomes, pathways, diseases and drugs, *Nucleic Acids Res.* 45 (D1) (2017) D353–D361.
- [11] M. Pomaznoy, B. Ha, B. Peters, GOnet: a tool for interactive Gene Ontology analysis, *BMC Bioinf.* 19 (1) (2018) 470.
- [12] D. Szklarczyk, et al., STRING v11: protein-protein association networks with increased coverage, supporting functional discovery in genome-wide experimental datasets, *Nucleic Acids Res.* 47 (D1) (2019) D607–D613.
- [13] D. Szklarczyk, et al., The STRING database in 2017: quality-controlled protein-protein association networks, made broadly accessible, *Nucleic Acids Res.* 45 (D1) (2017) D362–D368.
- [14] N.T. Doncheva, et al., Cytoscape StringApp: network analysis and visualization of proteomics data, *J. Proteome Res.* 18 (2) (2019) 623–632.
- [15] C.H. Chin, et al., cytoHubba: identifying hub objects and sub-networks from complex interactome, *BMC Syst. Biol.* 8 (Suppl 4) (2014) S11.
- [16] Y. Ru, et al., The multiMiR R package and database: integration of microRNA-target interactions along with their disease and drug associations, *Nucleic Acids Res.* 42 (17) (2014) e133.
- [17] C. Chen, et al., Real-time quantification of microRNAs by stem-loop RT-PCR, *Nucleic Acids Res.* 33 (20) (2005) e179.
- [18] S. Chang, W. Chen, J. Yang, Another formula for calculating the gene change rate in real-time RT-PCR, *Mol. Biol. Rep.* 36 (8) (2009) 2165.
- [19] Y. Hochberg, Y. Benjamini, More powerful procedures for multiple significance testing, *Stat. Med.* 9 (7) (1990) 811–818.
- [20] A.R. Perestrelo, et al., Multiscale analysis of extracellular matrix remodeling in the failing heart, *Circ. Res.* 128 (1) (2021) 24–38.
- [21] L. Colucci-D'Amato, L. Speranza, F. Volpicelli, Neurotrophic factor BDNF, physiological functions and therapeutic potential in depression, neurodegeneration and brain cancer, *Int. J. Mol. Sci.* 21 (20) (2020).
- [22] K. Duspara, et al., Targeting the Wnt signaling pathway in liver fibrosis for drug options: an update, *J Clin Transl Hepatol* 9 (6) (2021) 960–971.
- [23] H. Yamakawa, et al., Thyroid hormone plays an important role in cardiac function: from bench to bedside, *Front. Physiol.* 12 (2021) 606931.
- [24] S.E. Honeycutt, et al., Netrin-1 Directs Vascular Patterning and Maturity in the Developing Kidney, *Development*, 2023.
- [25] K. Zhang, et al., Asporin is a potential promising biomarker for common heart failure, *DNA Cell Biol.* 40 (2) (2021) 303–315.
- [26] S. Deckx, S. Heymans, A.P. Papageorgiou, The diverse functions of osteoglycin: a deceitful dwarf, or a master regulator of disease? *Faseb. J.* 30 (8) (2016) 2651–2661.
- [27] K.V. Engebretsen, et al., Lumican is increased in experimental and clinical heart failure, and its production by cardiac fibroblasts is induced by mechanical and proinflammatory stimuli, *FEBS J.* 280 (10) (2013) 2382–2398.
- [28] W. Guo, et al., Osteomodulin is a potential genetic target for hypertrophic cardiomyopathy, *Biochem. Genet.* 59 (5) (2021) 1185–1202.
- [29] P. Lefebvre, et al., Interspecies NASH disease activity whole-genome profiling identifies a fibrogenic role of PPARalpha-regulated dermatopontin, *JCI Insight* 2 (13) (2017).
- [30] J. Nishiu, T. Tanaka, Y. Nakamura, Identification of a novel gene (ECM2) encoding a putative extracellular matrix protein expressed predominantly in adipose and female-specific tissues and its chromosomal localization to 9q22.3, *Genomics* 52 (3) (1998) 378–381.
- [31] H.B. Wang, et al., Deletion of microfibrillar-associated protein 4 attenuates left ventricular remodeling and dysfunction in heart failure, *J. Am. Heart Assoc.* 9 (17) (2020) e015307.
- [32] X. Wei, et al., Myocardial hypertrophic preconditioning attenuates cardiomyocyte hypertrophy and slows progression to heart failure through upregulation of S100a8/A9, *Circulation* 131 (17) (2015) 1506–1517, discussion 1517.
- [33] H. Tsujioka, et al., Impact of heterogeneity of human peripheral blood monocyte subsets on myocardial salvage in patients with primary acute myocardial infarction, *J. Am. Coll. Cardiol.* 54 (2) (2009) 130–138.
- [34] M. Liu, et al., G protein-coupled receptor FPR1 as a pharmacologic target in inflammation and human glioblastoma, *Int. Immunopharm.* 14 (3) (2012) 283–288.